Fuel 304 (2021) 121370

Contents lists available at ScienceDirect

Fuel

journal homepage: www.elsevier.com/locate/fuel

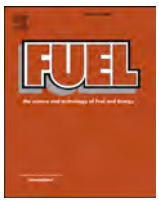

Full Length Article

Emission prediction and analysis on CH_4/NH_3/air swirl flames with LES-FGM method

Zhenhua An [a], Meng Zhang [a,*], Weijie Zhang [a], Runze Mao [a], Xutao Wei [a], Jinhua Wang [a], Zuohua Huang [a], Houzhang Tan [b]

[a] State Key Laboratory of Multiphase Flow in Power Engineering, Xi'an Jiaotong University, Xi'an 710049, China
[b] MOE Key Laboratory of Thermo-Fluid Science and Engineering, Xi'an Jiaotong University, Xi'an 710049, China

ARTICLE INFO

Keywords:
Large eddy simulation
Hydrogen carrier
Ammonia
NOx emission
Swirl flame

ABSTRACT

Ammonia, made up of 17.8% hydrogen, is one of carbon free fuels which can be used in large-scale power plants. However, ammonia combustion faces some challenges due to the high NOx emission. This study investigates the emission characteristics of CH_4/NH_3/air co-firing premixed swirling flames with NH_3 mole fraction up to 60% in a model combustor. Large eddy simulation (LES) coupled with flamelet generated manifold (FGM) model which considers the transport equations of slow chemical emission component was performed, with experimental validation in both flame structure and global emission. The simulation shows an overall good agreement with experimental results. It is found that the NO emission is improved with the NO transport equation calculated during the simulation. The results imply that the nitrogenous components, residence time and temperature are important factors that influence NO concentration profile. The residence time of inner recirculation indicates the NO level for CH_4/NH_3/air flames, and local high NO concentration is mainly caused by local long residence time. The OH and NO are correlative in premixed CH_4/NH_3/air flames because these components are both strongly related to the temperature. N_2O has a correlation with NH and HNO components. The radical components such as HNO, O, OH etc. also influence the emission formation process. When the NH_3 ratio is closed to 40%, the concentration of H, OH, O2 and HNO are all adequate to produce maximum NO.

1. Introduction

Ammonia (NH_3), identified as a suitable hydrogen carrier, is one of the most important potential energy resources in the hydrogen energy system facing the zero/low-carbon economy since it is a carbon-free molecule. [1–3]. Moreover, ammonia is made up of 17.8% hydrogen by weight thus has a considerable energy capacity. It can be stored in liquid at the pressure of 0.8 bar at room temperature or under −33 ℃ at atmospheric pressure [3,4], presenting an easier storage feature comparing with methane (CH_4). Recent investigations [3,5,6] show that ammonia is not only an attractive long-term solution for carbon neutrality but also can play a strategic role in the transition phase. The CO_2 footprint can be progressively lowered by shifting from fossil-based fuel to ammonia [7]. Therefore, the application of ammonia in the large scale power plants becomes one of the main objectives for the ammonia research community.

The strategy using ammonia as the fuel in gas turbines is not a new concept. US army engineer research and development Laboratories developed a gas turbine fueling with ammonia as early as 1966 [8]. However, the project was abandoned due to its unfriendly combustion properties. The main challenges of applying ammonia in gas turbines are attributed to the extremely low laminar burning velocity, causing a badly stable combustion range, and high nitrogen content resulting in high NOx emissions. Ammonia was seldom considered as a fuel due to these challenges, since the global climate issue caused by carbon emissions was not prominent in the past few decades. However, motivated mostly by the need to understand the combustion process and chemistry, a number of researches on ammonia combustion were initiated.

Recent studies [6,7,9] show that one of the effective ways to enhance the flame stabilization limits in a gas turbine combustor is to carry out the co-firing strategy of NH_3/CH_4 or NH_3/H_2 since the flame speed and heat release rate are increased [10,11]. This strategy also provides a transitional approach shifting the energy resource from carbon-base to carbon-free to achieve low-carbon emission. However, large amounts of

* Corresponding author.
E-mail address: mengz8851@xjtu.edu.cn (M. Zhang).

https://doi.org/10.1016/j.fuel.2021.121370
Received 3 May 2021; Received in revised form 21 June 2021; Accepted 30 June 2021

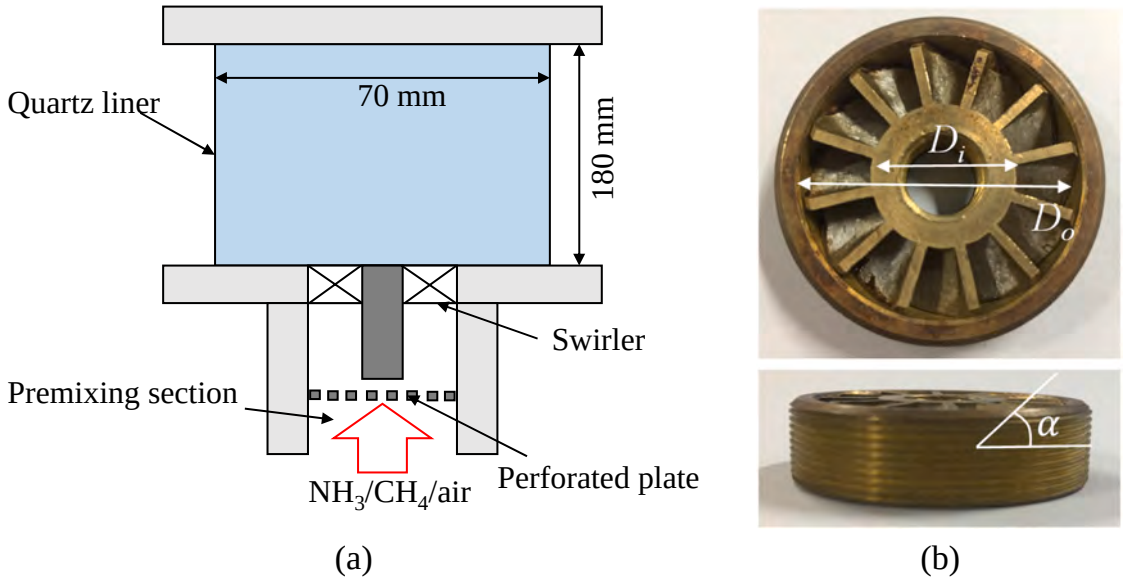

Fig. 1. (a) The head section of the swirl combustor; (b) the used swirler.

NOx will be produced by the co-firing combustion because of the cross chemical reaction of the fuel NOx chemistry in the meantime [5]. To compromise the flame stabilization and the emissions, several research groups attempted to find out intrinsic relation of the flame stabilization mechanism and the emission performance from the chemistry point of view [3,5,11].

Hayakawa et al. [4] investigated emission characteristics of ammonia/air premixed flames in a swirl combustor experimentally. They found that the NO emission decreased and ammonia concentration increased at fuel rich conditions. Significantly, an optimum equivalence ratio was found in rich condition where NO and ammonia emission were both low. Okafor et al. [12] investigated the emissions in micro gas turbine combustors fueled with CH_4/NH_3 co-firing fuels with laser diagnostics techniques and Fourier Transform Infrared (FTIR) gas analyzer. The rich-lean combustion strategy can realize significantly low emissions, i.e. 49 ppmv of NOx in their study. Kurata et al. [9,13] developed a NH_3 or CH_4/NH_3 fuel gas-turbine power generations. Their gas-turbine power generations can be operated over a wide range of power and rotational speeds, and the NO emission can be controlled by fuel rich or lean conditions and diluted air. The combustion performance was also largely studied by the numerical simulation due to its comprehensive information. Li et al. [6] analyzed the emission performance of NH_3/CH_4/air mixture combustion at gas turbine conditions using chemical reactor networks (CNR) numerically. The results showed that the main components of NOx is NO. The NOx emission can be controlled less than 30 ppm through two-stage combustion even when the fraction of NH_3 reached 40%. Somarathne et al. [14] investigated the emission characteristics of premixed NH_3/air swirl flames using large eddy simulation (LES). They found that NO emission and unburnt NH_3 emission decreased with an increase in pressure. The study also pointed out that low NO emission can be achieved by the secondary air injection system. Somarathne et al. [15–17] also investigated amounts of emission performances of NH_3 non-premixed combustion using LES with a finite-rate chemistry method. They found that both the temperature and OH concentration gradually decreased with the partial replacement of CH_4 with NH_3. The NO emissions had the similar trend with OH concentration at high temperatures.

For developing ammonia-fueled combustors, the accurate prediction of NOx formation of NH_3/CH_4 co-firing flame with different CH_4 blending ratios under various equivalence ratios is of primary importance. Instead of the computational expensive finite rate chemistry combustion models, such as thicken flame model or PaSR model, the flamelet generated manifold (FGM) method is quite effective for simulating various operating conditions. Only several transport equations of mass, momentum and control variables are need to solve. Honzawa et al. [18] used the FGM method to predict the NO and CO emissions of CH_4/NH_3/air combustion. They investigated the influence of wall heat losses due to radiation on the formation of NO and CO. The result showed that non-adiabatic FGM/LES method agreed much better than the adiabatic FGM/LES method with the experiments, indicating that the heat loss is non-negligible when simulating CH_4/NH_3/air combustion. However, the NO is a long formation process pollutant when seeking the chemistry of NO formation [19]. Transport effect is one of the essential issues when predicting the NO emission profile in the combustion chamber. Therefore, the prediction might be inaccurate by only retrieving NO value from FGM table directly. As the investigation from the literature [19], the prediction ability on NO concentration can be improved through adding extra transport equations.

To precisely capture the NOx emissions for CH_4/NH_3/air co-firing flames, the ammonia volume fraction up to 60% are investigated in a formerly used swirl combustor [20] using FGM/LES method coupled with detailed chemistry. The role of transport of NO species is studied for various conditions. It is worth emphasizing that this work is the further development of our previous research [20], which investigated the emission characteristics of CH_4/NH_3/air combustion based on the same swirl combustor. The target conditions of simulation in the current study is part of conditions in our previous research to extend the understanding of emission performance of CH_4/NH_3/air combustion. The flame structure and emission characteristics are measured using laser diagnostics techniques (PIV and OH-PLIF) and Gasmet DX4000 Fourier Transform Infrared (FTIR) gas analyzer. The flamelet generated manifolds (FGM) method containing heat loss is operated to investigate the emission characteristics of premixed swirl CH_4/NH_3/air flames [21]. We compared the prediction of NO emission with additional transport equation. The role of each effect is analyzed. The effects of flow structure on emission formation and the key radical components are also investigated.

2. Experimental setup

2.1. Configurations of swirl combustor and conditions

In this study, the experiments and simulations are operated on a model swirl combustor. The detailed structure of this combustor is

Table 1
Operating conditions summary.

Abbreviation	Composition	NH_3 blending ratio	equivalence ratio	U (m/s)	Vane angle
00NH3	CH_4/air	0	1.0	5	45°
20%NH3	NH_3/CH_4/air	0.2	1.0	5	45°
40%NH3	NH_3/CH_4/air	0.4	1.0	5	45°
60%NH3	NH_3/CH_4/air	0.6	1.0	5	45°

identified in our previous studies [20,22]. Fig. 1 (a) and (b) show the schematic of the combustor head section and the swirler with 12 vanes and 45 vane angle. The combustor includes a premixing section, a swirler and a quartz liner. CH_4, NH_3 and air are fully premixed in a mixing chamber. Then the mixture goes through a venturi nozzle and a perforated plate to prevent the propagation of downstream pressure waves and create the turbulence to the swirler. The turbulence parameters are measured by the hot wire anemometer experimentally. The swirl number S represents the intensity of the swirl motion and is calculated as follows:

$$S = \frac{2}{3}\frac{1-(D_i/D_o)^3}{1-(D_i/D_o)^2}tan\alpha \quad (1)$$

The swirl number is 0.71 in the current study. A squared liner equipped with quartz glass on four sides is used to view the flame and allow laser diagnostics. The dimension of squared liner is 70 × 70 × 180 mm^3. The components of the fuel mixture are methane and ammonia. The NH_3 fraction in the fuel, η_{NH3}, defined as Eq. (2)

$$\eta_{NH_3} = \frac{Q_{NH_3}}{Q_{CH_4} + Q_{NH_3}} \quad (2)$$

where Q_{CH_4} and Q_{NH_3} are the volume flow rate or the mole fraction of

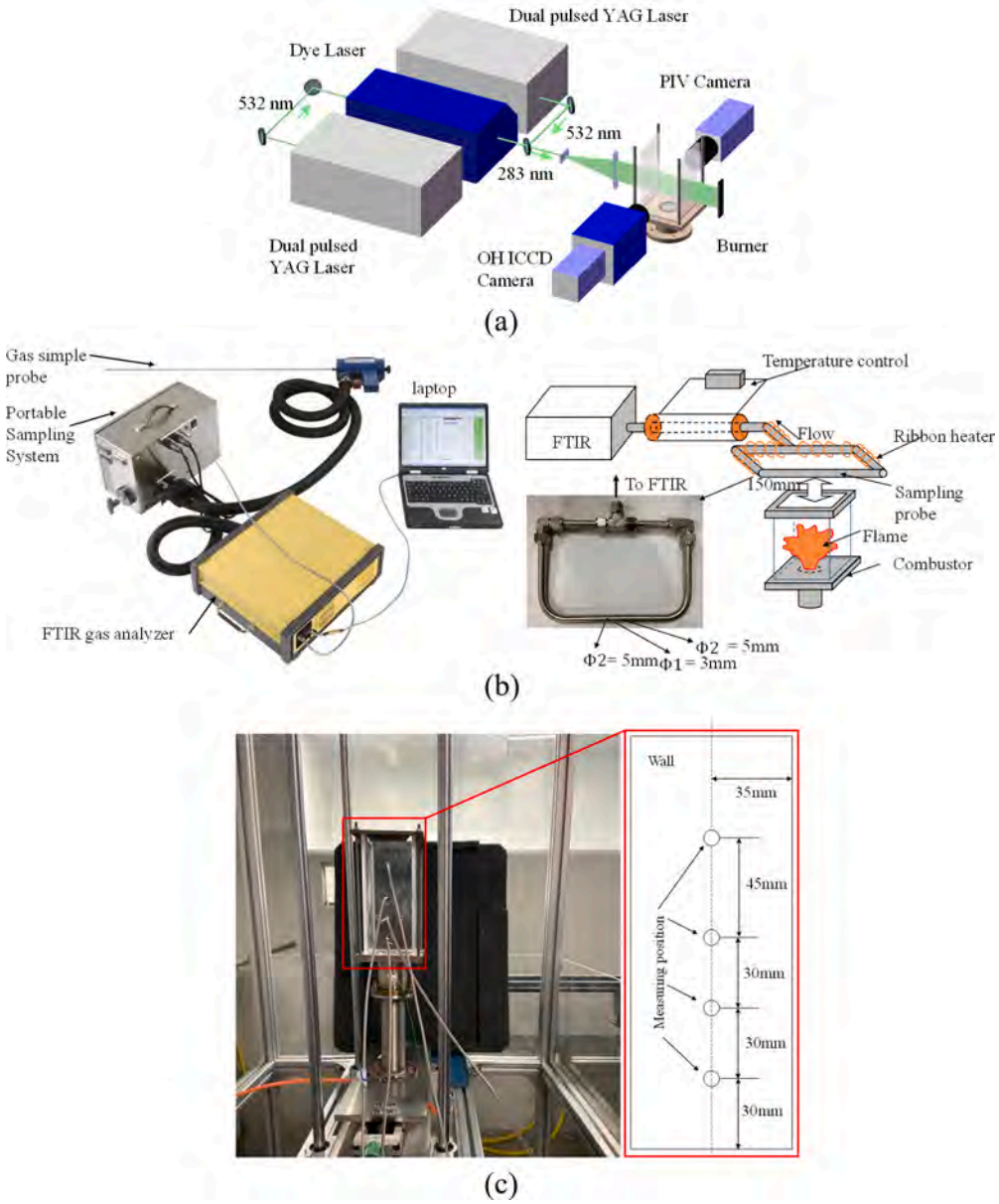

Fig. 2. (a) Laser diagnostics system (red dash box: PIV and blue dash box: OH-PLIF), (b) The FTIR system (lift) and the schematic of the measurement (right), (c) The experimental device and the measuring position of wall temperature. (For interpretation of the references to color in this figure legend, the reader is referred to the web version of this article.)

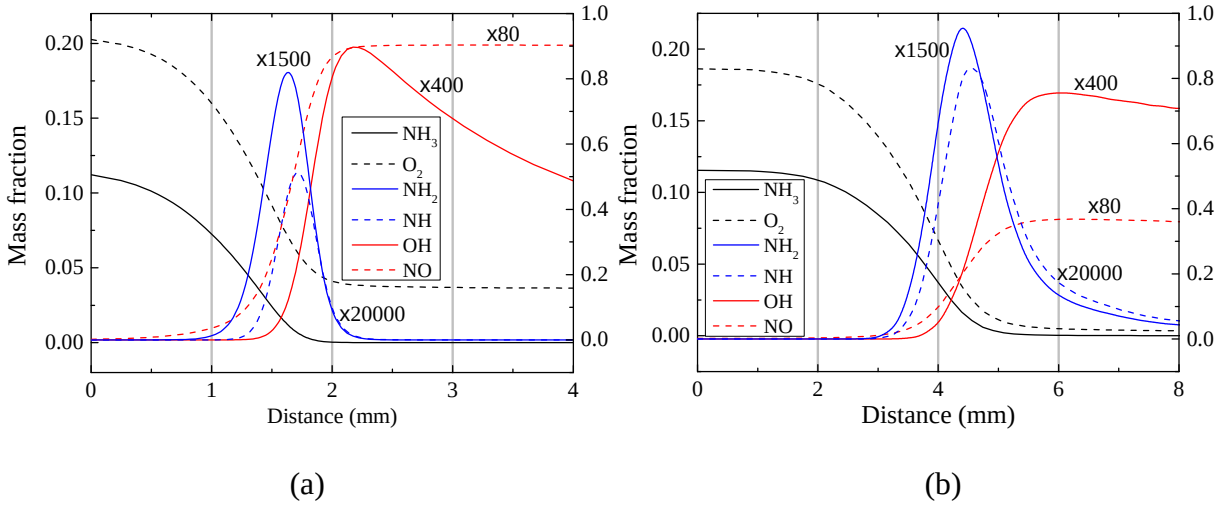

Fig. 3. The component values across the flamelet, (a) 1-D simulation, (b) LES-FGM simulation.

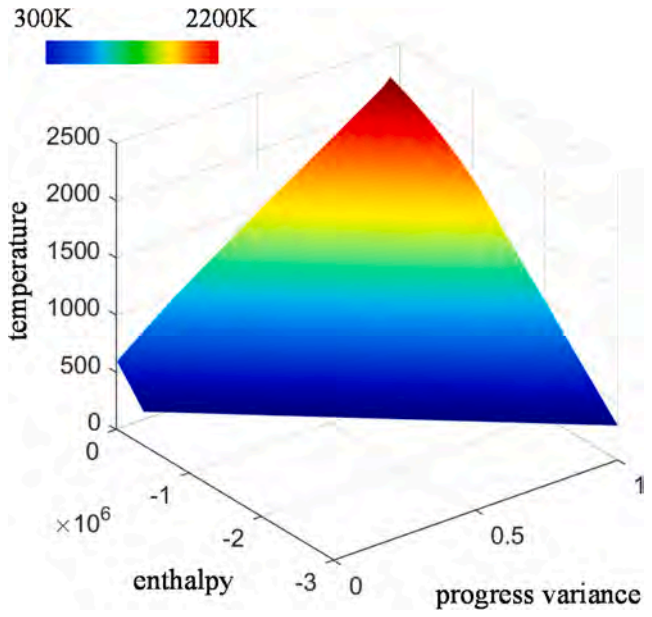

Fig. 4. Temperature (K) along the manifold.

methane and ammonia, respectively. η_{NH3} is up to 60% in the current study. The equivalence ratio of 1.0 is selected in current study which produces excessive NOx [20]. Therefore, there is more comparative value to investigate the mechanism of emission formation in this condition. The mean inlet velocity *U* is kept at 5 m/s for all conditions. The operating conditions are listed in Table 1. For brevity, the flames will be mentioned as their abbreviations in the following sections, as designated in Table 1.

2.2. Experimental equipment

In current study, the velocity field and OH profile representing the flame structure are measured by PIV and OH-PLIF techniques, respectively. Exhaust gas of CH_4/NH_3/air flames is measured by Gasmet DX4000 Fourier Transform Infrared (FTIR) gas analyzer.

The laser diagnostics system which consists of PIV and OH-PLIF is shown in Fig. 2 (a). The PIV system mainly includes a double-cavity Nd: YAG laser (Litron make), a double shutter CCD camera (Imager LX 2 M) and the data acquisition software. The source laser produces double pulse with a wavelength of 532 nm, 2 × 300 mJ pulse energy at a 10 Hz repetition rate. TiO_2 with a particle size of 0.5–1 μm is the seeding particle. The scattering is collected by the CCD with a macro lens (100 mm, F/2.8) at a working distance of 400 mm. The OH-PLIF system consists of a Nd: YAG laser (Quanta-Ray Pro-190), a pumped dye laser (Sirah PRSC-G-3000), an ICCD camera (LaVision Image ProX) and the data acquisition software. The source laser is produced at wavelength of 532 nm with 10 Hz and 5 W. And then the laser frequency is doubled with the pumped dye laser to excite OH fluorescence signal at a wavelength of 283 nm. The OH fluorescence is detected by an ICCD camera. The finest visualized field size is about 800 × 600 pixels, with the resolution is about 0.145 mm/pix.

The FTIR system consists of a gas analyzer and a Gasmet Portable Sampling System (PSS). Fig. 2 (b) shows the FTIR system and the schematic of the measurement. FTIR is an infrared spectrometer based on the principle of Fourier transform of infrared light after interference. The exhaust gas simple probe is made of high temperature resistant stainless steel tube which is located at 150 mm above the combustor outlet, and the temperature of sample probe is controlled by a ribbon heater to prevent water vapor from condensing along the pipeline. There are three holes in the middle of the stainless steel tube. The equipment is preheated to 453 K (180℃) firstly during the measurement. Then the background calibration is measured automatically by PSS with nitrogen. When the values of emissions get to steady state, the measured data is collected for statistical processing. In the measurement, the uncertainties are no larger than 50 ppmv for NO and NH_3 because the measuring range is 5000 ppm. However, the uncertainties are less than ± 10 ppm for CH_4, O_2, N_2O and NO_2 since the measuring range is less than 200 ppm. We tested the repeatability before the experiments and the relative error of the measurement is below 5% for the major species for the tested mixture. The accuracy of FTIR system was also introduced in our previous research [23].

The wall temperature is measured through four positions on the wall by thermocouple, and the experimental device is shown in Fig. 2 (c). The uncertainties of thermocouple are about 5%. After the temperature remains a certain value and the fluctuation is very small, we gather the statistical data for four position.

3. Numerical methodology

3.1. Flamelet generated manifold (FGM) methods

In this study, there is no fuel stratification in the premixed flame. Therefore, the flame is calculated by a 2D-FGM method in which the

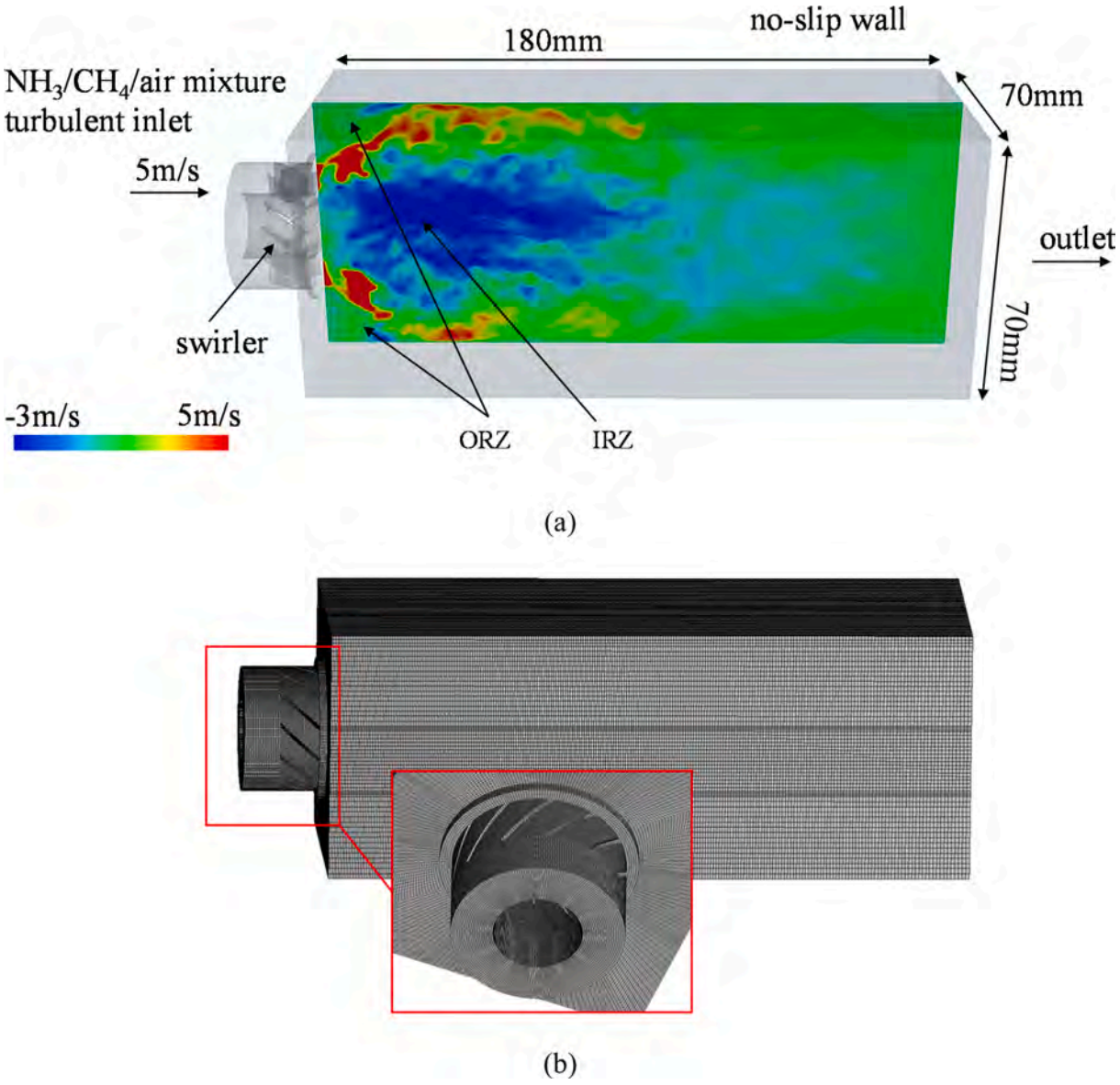

Fig. 5. (a) The computational domain with boundary condition, (b) mesh details.

Table 2
Boundary conditions summary.

Boundary	Thermal boundary conditions	Velocity boundary conditions
Inlet	Inlet of 300 K	LEMOS inflow
Swirl vane	Adiabatic	No-slip
Squared quartz liner	Isothermal wall	No-slip
Outlet	Adiabatic	Non-reflecting boundary

control variables are represented by the progress variance (PV, denoted by γ) and enthalpy (denoted by h). The progress variable is used to describe the transition from fresh mixture to burnt gas, which is defined as a linear combination of species mass fraction:

$$\gamma = \sum_{i=1}^{N_s} \alpha_i Y_i \tag{3}$$

where N_S is the total number of species, α_i are weighting coefficients which can be chosen arbitrarily, Y_i is the mass fraction of specie *i*. The monotonic profile of γ in the whole interval from the unburned mixture to the chemical equilibrium should be ensured. In this study, the α_i are defined similar with Donini et al. [24] $\alpha_{co2} = -100M_{CO_2}^{-1}$, $\alpha_{H2O} = -100M_{H_2O}^{-1}$, $\alpha_{H2} = -100M_{H_2}^{-1}$, $\alpha_{o2} = -100M_{O_2}^{-1}$ and $\alpha_i = 0$ for other species. *M* is the molecular weight of species *i*. This method can optimize the chemistry resolution. Fig. 3 shows the comparison between 1-D flamelet calculated by CHEMKIN PRO (a) and turbulent flamelet calculated by current FGM model (b). It can be seen that LES-FGM result shows the same trend with 1-D flame propagation although there are some discrepancies in value. It's indicated that although the current approach can capture the structure of the premixed flame even it doesn't include a model on capturing the flame propagation.

In order to fix the heat loss of the chamber wall, the enthalpy is considered. The specific enthalpy is adopted as one of the control variables to describe energy, which is defined as [25]:

$$h_i = h_i^{ref} + \int_{T^{ref}}^{T} c_{pi}(T')dT' \tag{4}$$

where h_i^{ref} is the enthalpy of formation at reference temperature T^{ref}, which is 300 K in the current study. c_{pi} is the specific heat capacity at

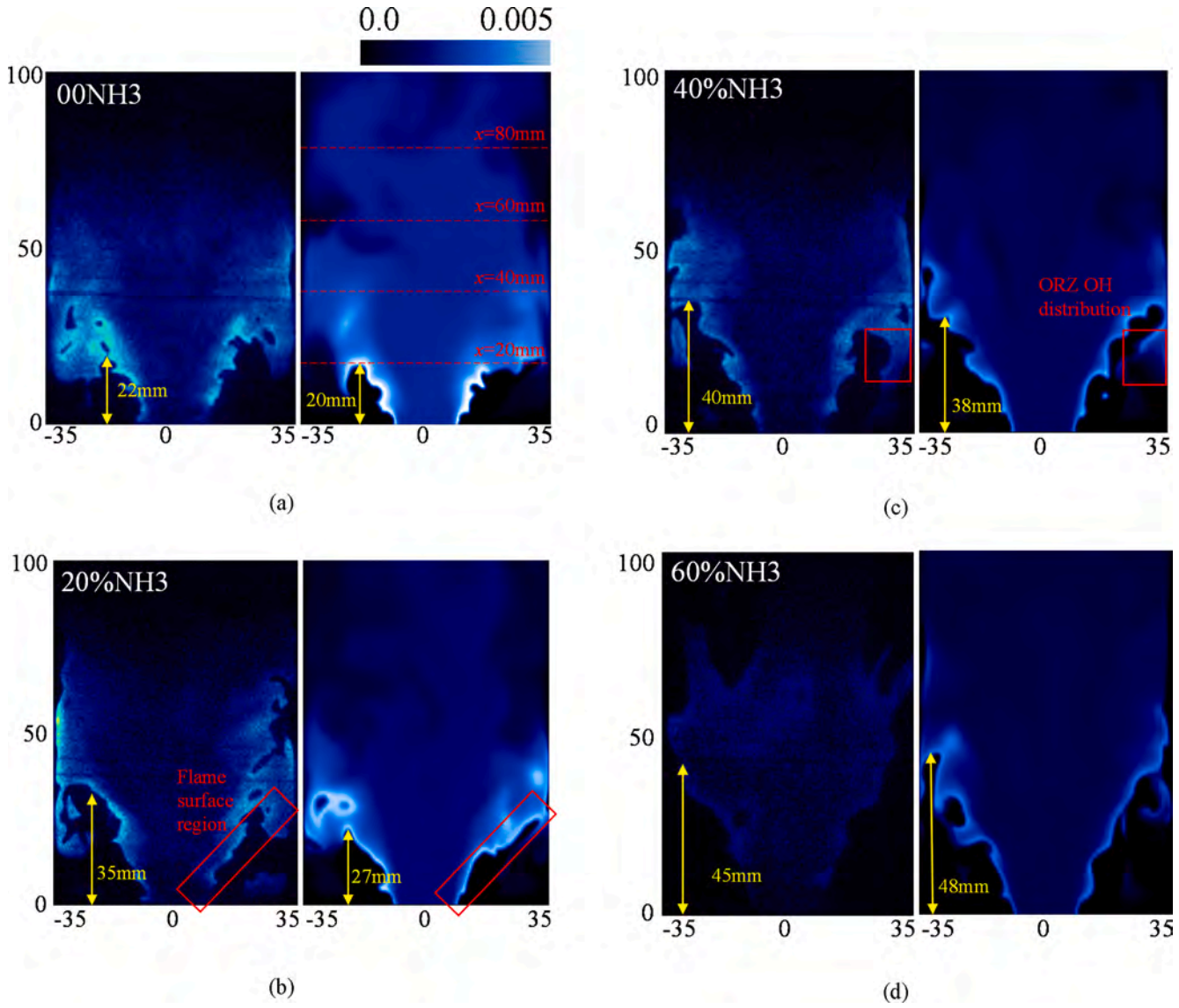

Fig. 6. Comparison of flame structure represented by OH-PLIF signal from experiment (left) and numerical OH distribution (right) for four different NH_3 fraction. (a) $00NH_3$, (b) $20\%NH_3$, (c) $40\%NH_3$, (d) $60\%NH_3$. Image dimensions are 70 × 100 mm.

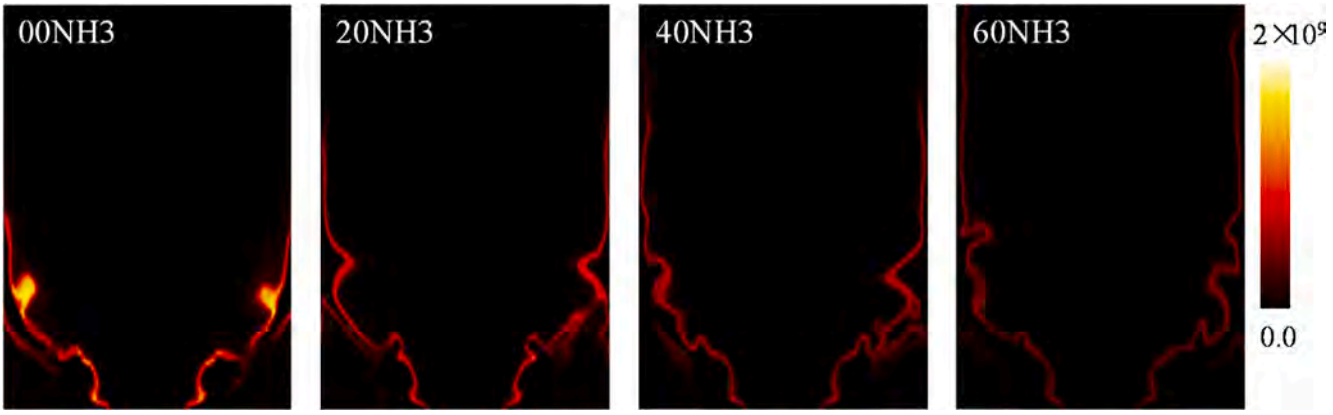

Fig. 7. The reduction of heat release rate of CH4/NH3/air flame with the NH3 ratio increasing.

constant pressure of species *i*.

A series of laminar flamelets are solved for different values of progress variance γ and enthalpy *h*, by introducing these two as control variables. The flamelet solutions are computed by methods of a 1D flame code, Chem1D [26], coupled with the reaction mechanism proposed by Okafor et al. [27]. The chemical mechanism consists of 368 elementary

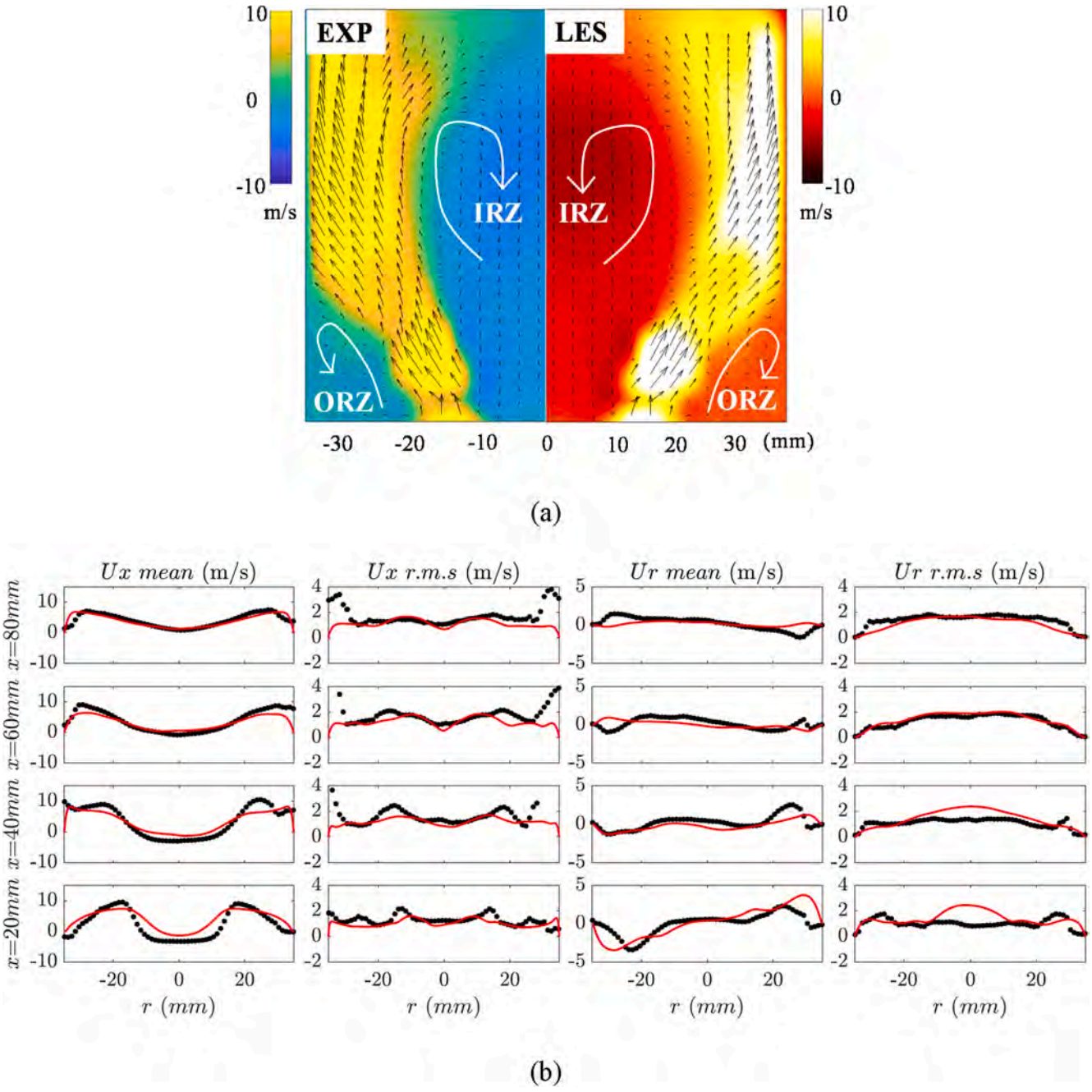

Fig. 8. Mean reacting flow velocity field of 60%NH3 flame. Left: the PIV measurement result; right: the LES result (a). Comparison of mean and r.m.s velocity profiles at different axial locations for (b) case 00NH3, (c) case 60%NH3. The black symbols and red solid lines indicate the results obtained from experimental measurement and computation, respectively. (For interpretation of the references to color in this figure legend, the reader is referred to the web version of this article.)

reactions between 59 species, which is verified to precisely capture the flame speed and ignition time as well as emission characteristics at various conditions [28]. Unity Lewis number is operated along the flamelets, neglecting differential diffusive effects since the Lewis number of CH_4/NH_3/air mixture is close to 1 [29].

Firstly, a steady, fully premixed flamelet is computed with inlet temperature of $T_u = 300$ K. At the burned side where chemical reaction is in equilibrium, Neumann type boundary conditions are imposed. Then, the heat losses of the laminar flamelets are solved for different values of enthalpy h at each equivalence ratio by the burner-stabilized flames at a constant Φ [24,30]. Furthermore, preheated flamelets with $T_u = 300 - 600$ K are also calculated to describe the preheating of the mixture. Finally, the thermochemical variables are mapped as a function of the control variables using these flamelet solutions. An overview of the resulting laminar manifold is shown in Fig. 4. The scalar variable (shown as temperature) is represented as a function of the progress variable and enthalpy value. The enthalpy is referenced to inlet condition where $h = 0$. The turbulence-chemistry interaction is considered for progress variable by method of top-hat function model, which is proposed by Floyd et al. [31]. There is no need to extend the database dimension in this model.

Then, the FGM tabulation can be coupled with the FGM solver based on OpenFOAM. In addition to the momentum and mass equations, transport equations for control variables are also solved. And the Sma-

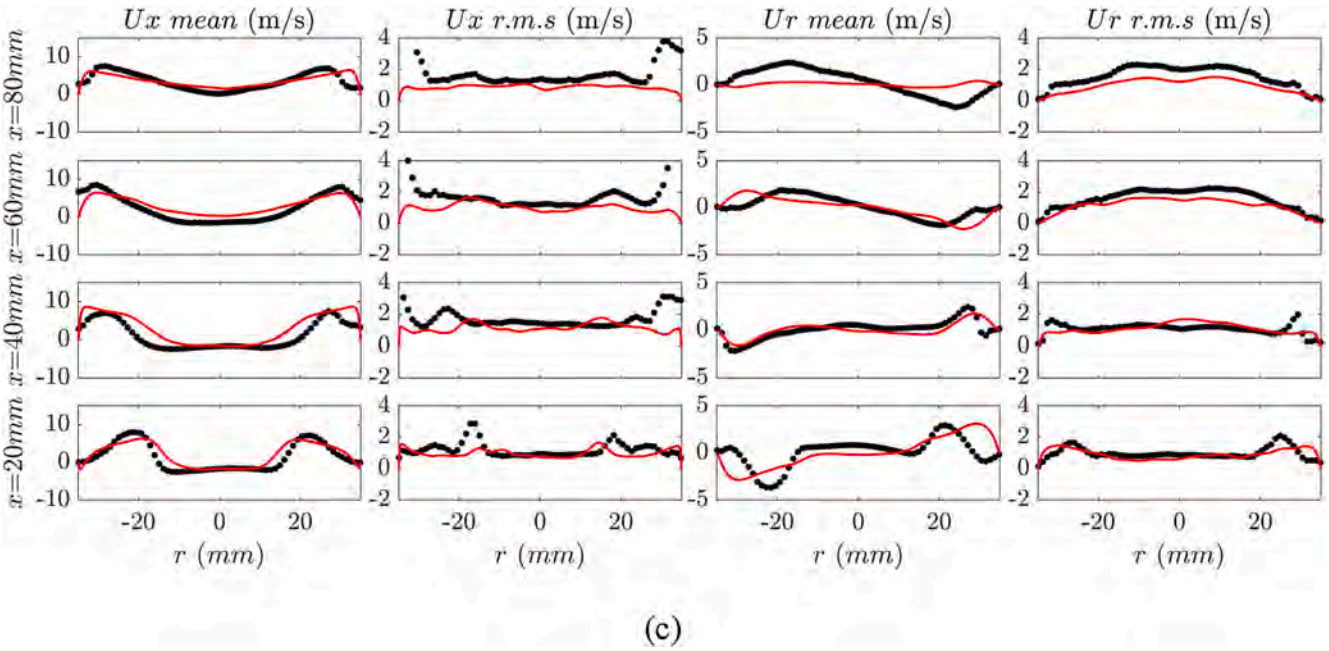

Fig. 8. (*continued*).

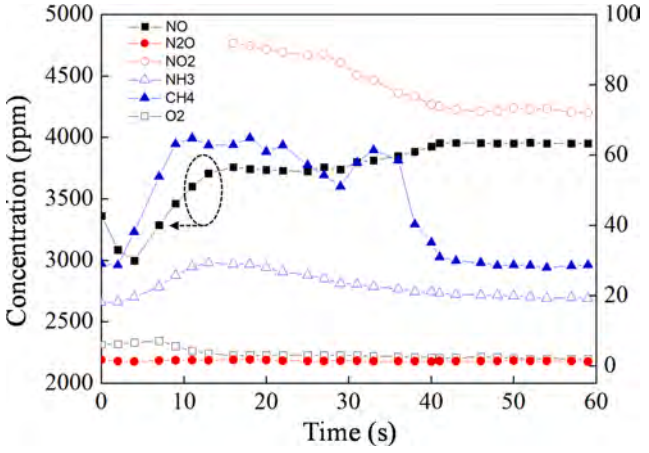

Fig. 9. The variation of the measured data against the time by FTIR.

gorinsky model [32] is adopted in order to close the non-linear terms of these equations. In this way, the transport equation of control variables can be written as [21]:

$$\frac{\partial}{\partial t}\left(\widehat{\rho}\widetilde{C_k}\right)+\frac{\partial}{\partial x_i}\left(\widehat{\rho}\widetilde{u}\widetilde{C_k}\right)=\frac{\partial}{\partial x_i}\left\{\left[\left(\frac{\widehat{\lambda}}{c_p}\right)+\frac{\mu_t}{Sc_t}\right]\frac{\partial\widetilde{C_k}}{\partial x_i}\right\}+\frac{\partial}{\partial x_i}\left(\widehat{d_{C_k}}\frac{\partial\widetilde{\gamma}}{\partial x_i}\right)+\widehat{\dot{\omega}_{C_k}} \tag{5}$$

The prediction of NO is difficult because of its slow formation rate compared with other species [19]. In this study, in order to predict the emission of NO better, an extra transport equation is solved for NO, which will be investigated in section 4.2.

3.2. Computational setup and procedure

The computational domain is the same with the experiment as shown in Fig. 5 (a). High quality structured hexahedral mesh is applied in this study. The number of cells of the current mesh is about 5 million. Higher grid density of cells is constructed in the flame region with cell size Δ less than 0.4 mm. The detail of mesh is shown in Fig. 5 (b). The mesh resolution is adequate for the current study, which is verified in our previous study [22,33]. All boundary conditions are summarized in the Table 2. The inlet turbulence is generated by the LEMOS inflow generator [34,35], generated by the perforated plate experimentally, with the prescribed spatial integral length scales, mean velocity and Reynolds stress tensor field. The isotropic turbulence at the inlet is assumed in simulation. The parameters of the LEMOS inflow generator are adjusted so that the mean and r.m.s velocity match the experimental data. It should also be noted that the turbulent inlet is placed 10 mm upstream of the vane swirler, so that the swirl turbulent flow field can be created and adjust to the combined effects of burner and swirler walls. A no-slip velocity boundary condition is specified at the burner and vane walls. For the outlet, the non-reflecting boundary condition is applied. Heat loss to the quartz glass walls is considered in the simulations by setting an isothermal temperature. The specific temperature of quartz glass walls for different NH_3 fraction cases is prescribed based on the experimental measurement, i. e. T_{00NH3} = 750 K, T_{20NH3} = 700 K, T_{40NH3} = 650 K, T_{60NH3} = 600 K. Other surfaces are set to be adiabatic which is fully indicated in our previous study [22].

The FGM solver is applied on OpenFOAM 2.3.x. The transport equations are advanced in time using a first-order implicit Euler scheme, and the time step is set 1×10^{-6} to keep the maximum Courant-Friedrich-Lewy (CFL) number less than 0.4 for all cases. The convection term is discretized by second order total variation diminishing (TVD) scheme Gauss limited Linear. For the scalar transport, the diffusion term is discretized by central differencing Gauss linear corrected. A PISO algorithm is used for pressure–velocity coupling. For all cases, the cold flow is calculated firstly, and then the reacting flow is calculated until reaching a steady state. The statistics are collected over 400 ms, which corresponds to more than 10 flow-through times (FTT), defined by the chamber length and inlet velocity. Simulations are performed on the Intel Xeon-E5 with 360 processors. Each case requires approximately 20,000 CPU hours.

4. Results and discussions

4.1. Comparison of flame structures and velocity fields

The prediction of flame structure is essential since it represents the distribution of radical species and temperature. Therefore, the emission

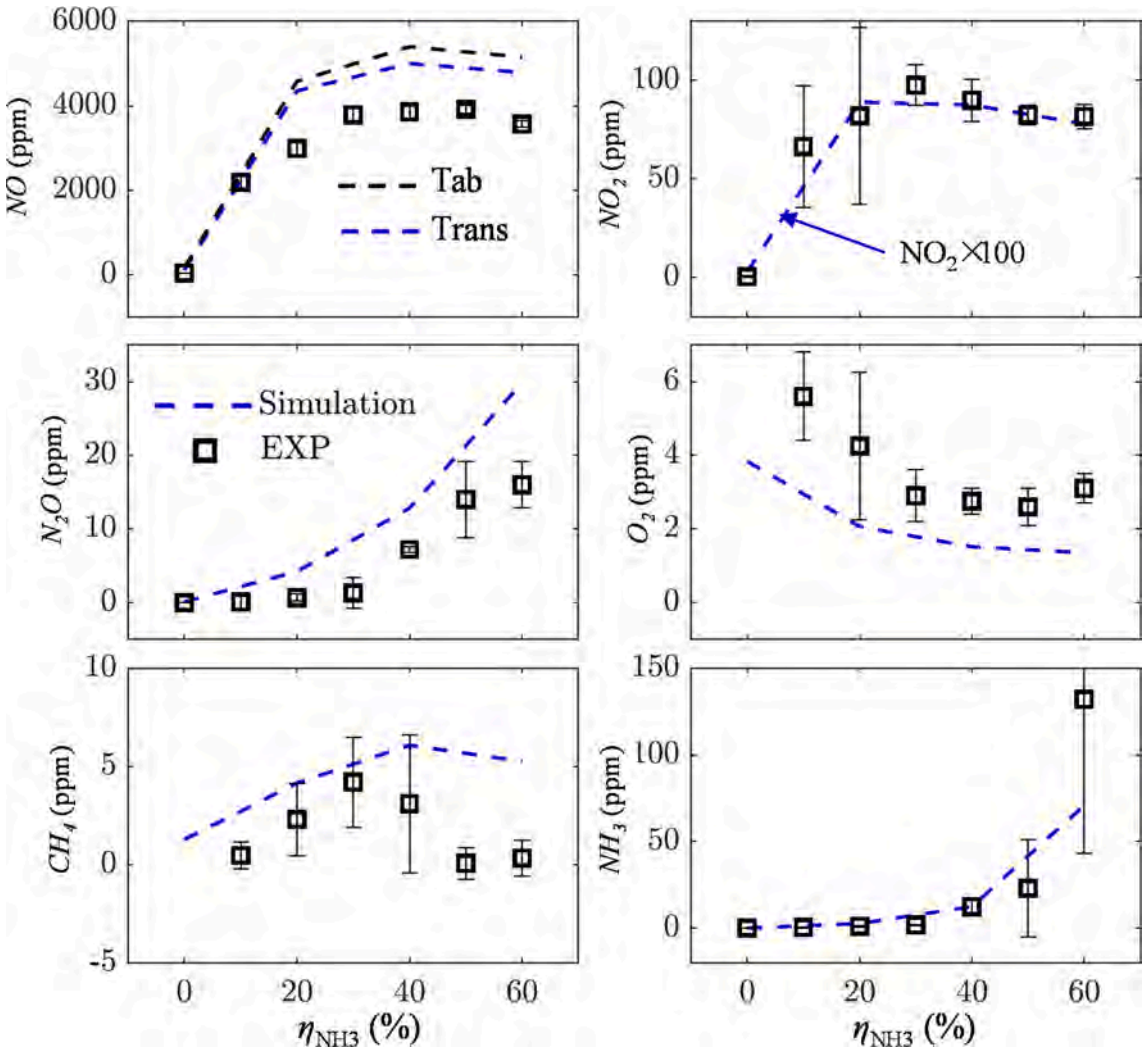

Fig. 10. Emissions of NO, NO_2, N_2O and O_2 concentration and unburnt fuel (CH_4 and NH_3) obtained from experiments and simulations as a function of NH_3 fraction. In figure of ppm_{NO}, the blue dash line is calculated from transported method and black dash line is tabulated value. (For interpretation of the references to color in this figure legend, the reader is referred to the web version of this article.)

characteristics could be highly related to the flame structure. Fig. 6 shows the comparison of OH species profile between the experimental measurements by OH-PLIF technique and LES simulation, for different NH_3 fraction, i.e. (a) $00NH_3$, (b) $20\%NH_3$, (c) $40\%NH_3$, (d) $60\%NH_3$. It can be clearly seen that with the increasing of NH_3 fraction, the OH-PLIF image intensity is reduced. For $00NH_3$ case, the sharp increase of OH intensity in the vicinity of flame surface region is marked in Fig. 6 (b), which can be regarded as the reaction location of premixed flames [36]. However, for $60\%NH_3$ case, the intensity of OH is non-significant. The weaker OH signal does not necessary imply the low combustion intensity. Therefore, the heat release rate (HRR) for all cases is investigated. It can be seen from Fig. 7 that the HRR decreases with the increasing of NH_3 ratio. Therefore, the combustion intensity is getting low when blending more NH_3 in CH_4/NH_3/air flame. Flame height is an essential factor to describe the macro flame structures, which is measured according to Singh's definition [37]. To be specific, the flame height is defined as the boundary of reaction zone which can be clearly demonstrated by the mean OH distribution. As a result, we used the mean OH figure to compare the height of flame. Fig. 6 shows the flame height for different η_{NH3} from experiment and simulation. It can be seen that with the increasing of η_{NH3} in the fuel, the flame height is getting longer. This is caused by the decreasing flame speed as the content of NH_3 increases [20,27], such that the flames can be only stabilized at a much more downstream location. There are some discrepancies between experiment and simulation. First, because the instantaneous images are compared, so the detail of flame construction will have some difference. However, the characteristics of the flames are captured, such as the outer recirculation zone. The other reason of discrepancies may be the influence of the Smagorinsky turbulent model. It is readily seen that the two remarkable phenomena, i.e. the decreasing of OH intensity and increasing of flame height with η_{NH3} are perfectly captured by FGM-LES numerical method. Furthermore, the OH distribution in outer recirculation zone (ORZ, which is shown in Fig. 5 (a) schematically) is also captured by the simulation. This achievement provides the fundament for investigation on emission prediction in following sections.

The experimental and LES results of mean reacting flow velocity fields are included in Fig. 8 (a). which shows the simulation can predict the reacting velocity fields well. The overall features of the velocity field are shown for both methods. The location, the shape and the scale of the inner recirculation zone (IRZ)/outer recirculation zone (ORZ) are clearly and accurately predicted by the LES simulation. For further quantitative comparison, the mean and root-mean-square (r.m.s) velocity between experimental measurement and simulation are presented. The results for $00NH_3$ and $60\%NH_3$ are displayed here and the velocity comparison for $20\%NH_3$ and $40\%NH_3$ is omitted for brevity. The velocity profile is extracted from four different axial locations, i.e.

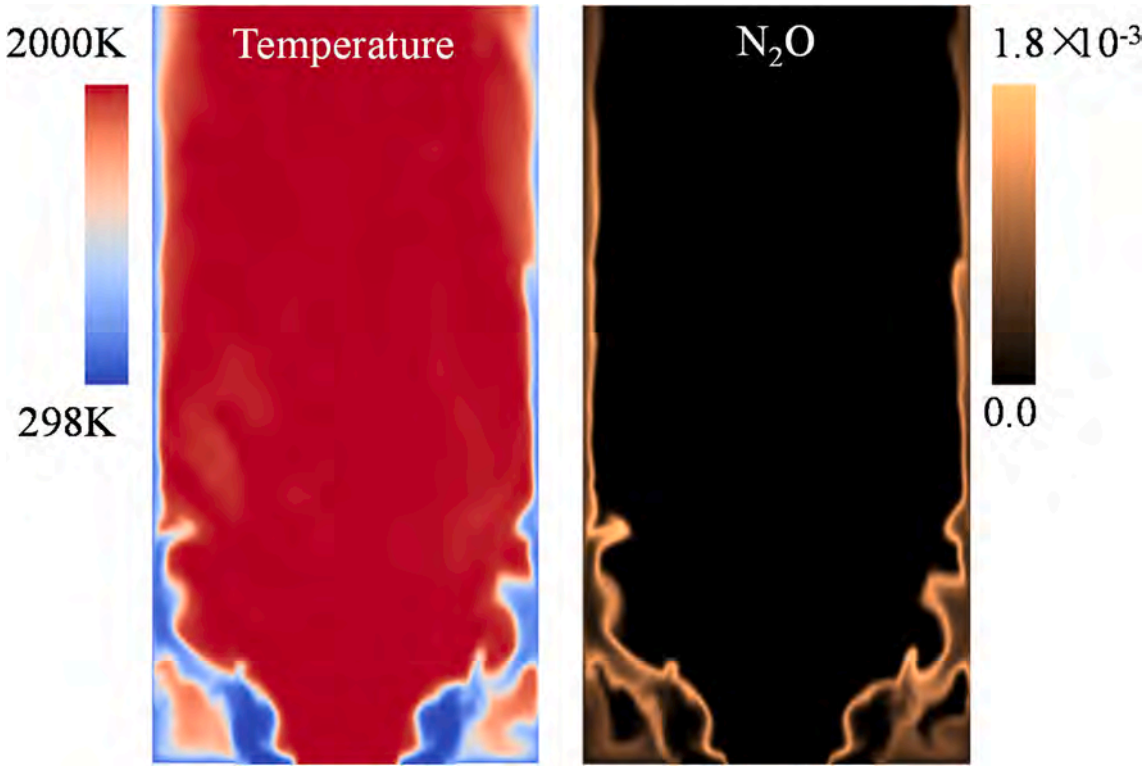

Fig. 11. The temperature and N_2O of the combustion zone for 60NH3.

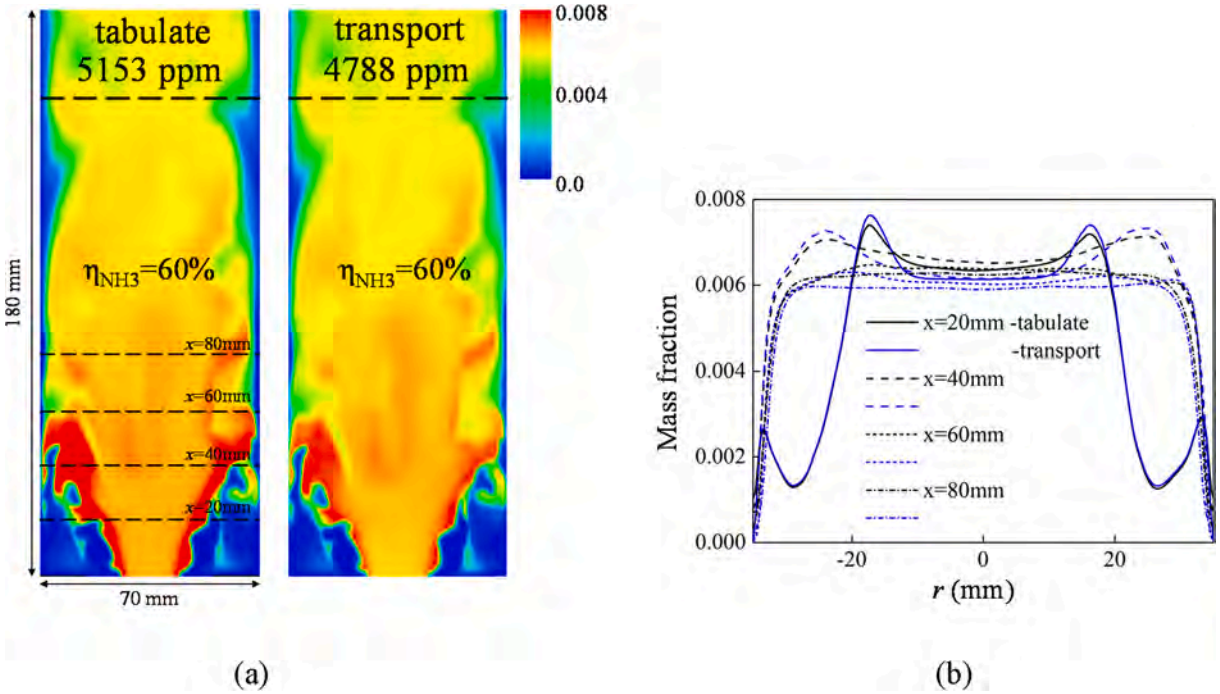

Fig. 12. Comparison of space and time average emissions (STAE) of NO between transported value and tabulated value with experiments. (a) The comparison of tabulated NO (left) and transported NO (right) distribution for case 60%NH_3, the STAE value of NO is also marked as ppm of mole fraction at the exit of burner. (b) The value of NO at different axial locations for case 60%NH_3.

$\times$ = 20 mm, x = 40 mm, x = 60 mm and $\times$ = 80 mm, which is shown in Fig. 8 (b). An overall satisfied agreement is achieved between the experiment and simulation for all cases.

The mean and r.m.s velocity of 00NH_3 at different axial locations are shown in Fig. 8 (b). It can be clearly seen that at the upstream location, i.e. x = 20 mm and x = 40 mm, negative mean axial velocity is captured, indicating the presence of the recirculation zone. The r.m.s velocity of simulation in axial direction is also well matched with the experiment. The peak value of r.m.s velocity at r=±20 mm is corresponding to the mixing layer between fresh mixture and inner recirculation zone (IRZ),

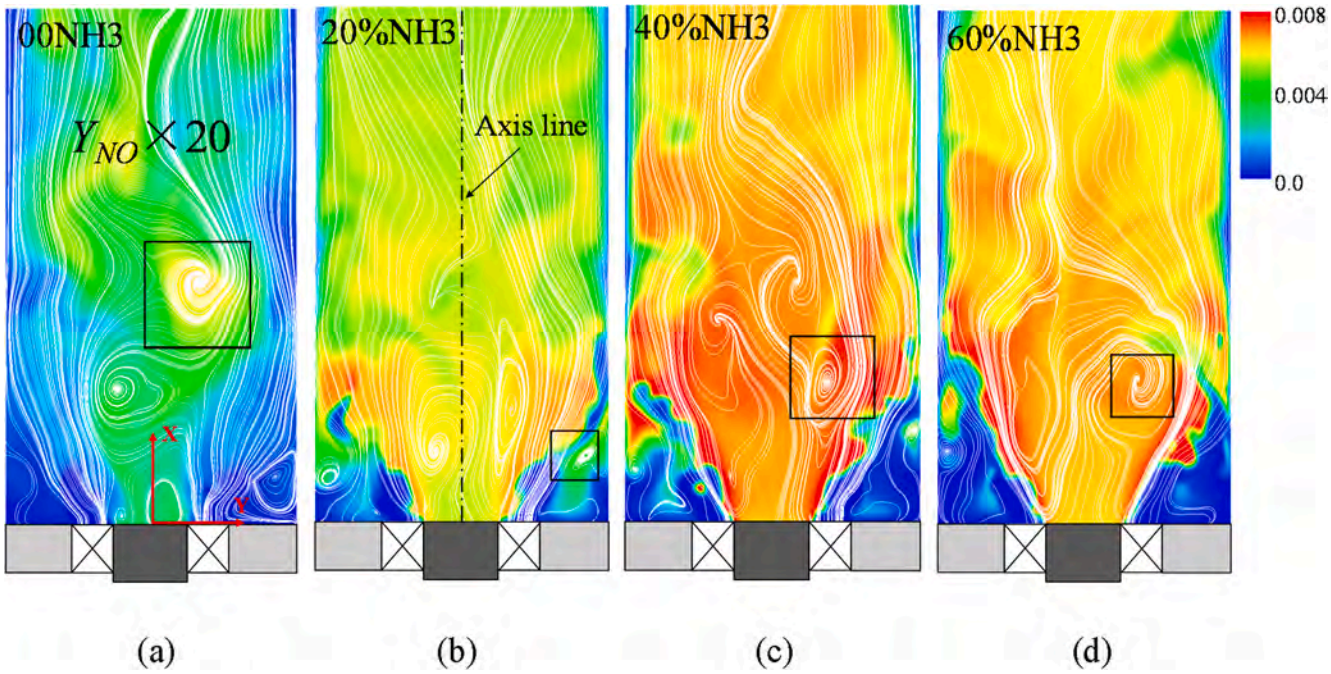

Fig. 13. Instantaneous NO distribution field coupled with the streamlines for different NH_3 fraction using the same color bar. (a) 00NH3, (b) 20%NH3, (c) 40%NH3, (d) 60%NH3. Image dimensions are 70 × 120 mm. (For interpretation of the references to colour in this figure legend, the reader is referred to the web version of this article.)

defined as the inner shear layer. Similarly, the mixing layer between fresh mixture and outer recirculation zone (ORZ) is defined as the outer shear layer. For the mean radial velocity, a large discrepancy is found at $x = 20$ mm, which can be partly caused by the uncertainties of experimental measurements. It also can be seen that radial r.m.s velocity shows a good agreement with the experiment measurement. As for the 60%NH_3 case shown in Fig. 8 (c), the velocity field is also captured well by simulation. The well agreements are achieved in Fig. 6 and Fig. 8 indicating the good capability of predicting the chemistry, flow dynamics and the proper specifications of the boundary conditions of our numerical simulation.

4.2. Emission prediction and the effects of NO transport equation

In order to predict NO emission, a main component of NOx with a low formation, two methods for calculating these species using FGM are compared. The first one is that the mass fraction of NO is directly retrieved from the FGM tabulation data, namely tabulated method. The other one is that calculating the NO concentration through extra transport equations, namely transported method. The transport equation of NO is shown as:

$$\frac{\partial}{\partial t}\left(\widetilde{\rho Y_{NO}}\right)+\frac{\partial}{\partial x_i}\left(\widetilde{\rho u Y_{NO}}\right)=\frac{\partial}{\partial x_i}\left\{\left[\left(\frac{\widehat{\lambda}}{c_p}\right)+\frac{\mu_t}{Sc_t}\right]\frac{\partial \widetilde{Y_{NO}}}{\partial x_i}\right\}+\left(\frac{\widehat{\dot{\omega}^c_{NO}}}{Y^{tab}_{NO}}\right)+\widehat{\dot{\omega}^p_{NO}} \tag{6}$$

where the source term of NO is directly looked up from the FGM tabulation database. In this method, the production and consumption of NO are given by the manifold. The overall amount of the mass fraction is computed by the transport equation. This method has been proved to improve the accuracy of NO prediction in the CH_4/air flame [19].

To validate the global emission of the numerical methods. The emission is measured by FTIR at 150 mm above the combustor outlet experimentally. Fig. 9 shows variation of the measured data against the time. It can be seen that the value will be stable after 40 s, after which the measured data is collected over 20 s. The mean value of statistical result is taken as global emission value. In simulation, the space and time-averaged emission (STAE) values in units of ppm are obtained by averaging the outlet plane of the combustor.

Emissions of NO, NO_2, N_2O, O_2 concentration and unburnt fuel (CH_4 and NH_3) obtained from experiment and simulation as a function of NH_3 fraction are shown in Fig. 10. The error bar calculated from the deviation of experimental measurement is also shown. It is observed that the simulation predictions on the concentration of emissions and unburnt fuels show very close trend with experiment. Some of the results even show a quantitative consistency. For the value of NO, the blue dash line is calculated from transported method and black dash line is obtained from the tabulated value. It can be clearly seen that the trend of variety is captured by the simulation. As for 00NH_3 there is nearly no NO emission, and the peak value of NO occurs at 40%NH_3. This phenomenon will be further investigated in section 4.4. Moreover, the magnitude value is also predicted by simulation, even with some discrepancy. The maximum relative error of NO concentration is less than 45%. The main source of NOx emission is NO, therefore, the NO emission is mainly considered in following content. The trend of NO_2 is also captured by simulation, which is first increased and then decreased. And the magnitude value is similar when the numerical result is expanded 100 times. The value of NO_2 is relatively low compared with experimental value. It is because that the reaction path of NO_2 was not optimized in the Okafor mechanism [27], resulting in inaccurate prediction on NO_2. For the value of N_2O, the trend and magnitude value are captured well by simulation. Fig. 10 also shows that O_2, CH_4 and NH_3 species are well predicted by simulation, and both the trend and the value are captured. FGM method principally uses quasi-steady state approximation for fast chemical processes. Therefore, the approach is well suited to predict free radical species such as O_2, CH_4 and NH_3.

In order to investigate the N_2O formation, Fig. 11 shows the temperature and N_2O of the combustion zone for 60NH3 case as example. It can be found that there is no N_2O distribution in IRZ where the temperature is high. It is indicated that N_2O is destroyed by high temperature profiles across the flame. Moreover, the N_2O is over predicted as shown in Fig. 10. The reason is that the mechanism has some discrepancies to predict N_2O and the FGM has some hypothesis which has two control variables to predict the other field.

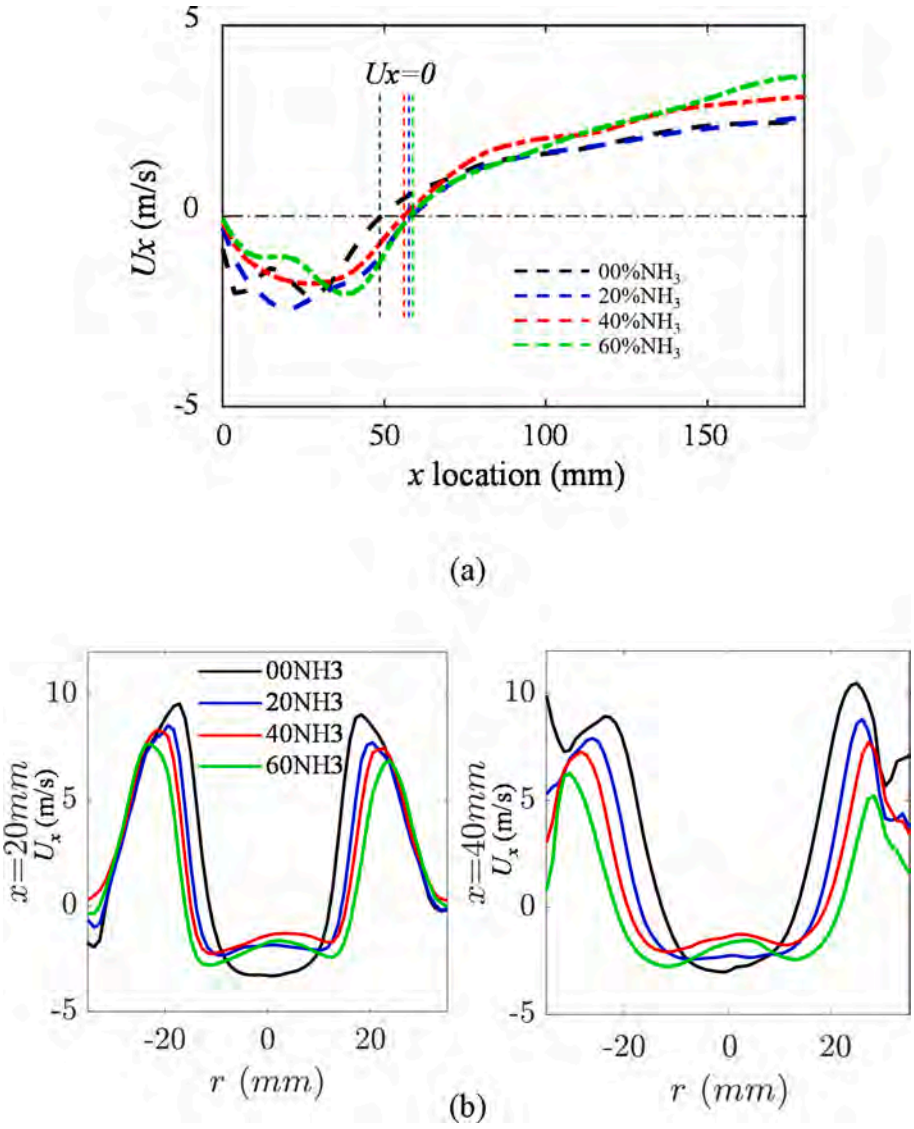

Fig. 14. (a) The numerical mean velocity of x direction along the axis line. (b) The experimental measurement of recirculation zone mean velocity (x = 20 mm and x = 40 mm).

The deviations of emission prediction may be caused by the fact that the mixture fraction, which can describe diffusion effect, is ignored in the simulation. In experiment, the fresh air maybe enters into the chamber from the crevice of quartz liner. The definition of progress variable is also a reason which can cause over prediction, and the deviations are also investigated by Samiran et al. [38]. However, the discrepancy can be accepted because the trend is captured well, and it is difficult to make sure that the simulation is absolutely same with the experiment.

In order to further identify the differences between two methods of NO calculation, Fig. 12 shows the comparison of STAE of NO between tabulated value and transported value with experiments. In order to investigate the difference of NO distribution, the NO field of 60%NH_3 is shown as example in Fig. 12 (a), with tabulated value and transported value. The STAE value of NO is also marked as ppm of mole fraction at the exit of burner, which is shown by black dash. The total NO value calculated by transported method is smaller than tabulated value. NO profile at different axial locations is shown in Fig. 12 (b). It can be clearly seen that the difference is mainly caused by the lower prediction in the inner recirculation zone. The reason of this discrepancy is that the generation of NO is a long chemical process, as it takes place through a great variety of reactions (NH2 → NH → NNH → HNO → NO). The reaction time scale is relatively long, and similar to the flow time scale. Therefore, the concentration of NO cannot be calculated correctly only by several control variables through infinite rate chemical tabulated method, and the species transport effects should not be ignored. Adding extra transport equation can consider the heat loss and species transport effects more comprehensively, which will increase the prediction accuracy of slow chemical substances.

4.3. *Effects of flow structure on emission formation*

The formation of emission is closely related with the flow within the combustion chamber, since NO is influenced by transport. In the experimental investigation, only the global emission characteristics can be captured in a regular way. Very few studies can provide the quantitative measurement at a single point [39]. To the best knowledge of the authors, there is no simultaneous quantitative 2D measurement of NO and the velocity field. Therefore, in this case high precision LES research can give full play to reveal the relationship between flow and pollutant formation.

To investigate the influence of flow field on emission formation, the instantaneous NO field coupled with the streamlines for NH_3/CH_4/air flames at different NH_3 fraction are shown in Fig. 13. The region of

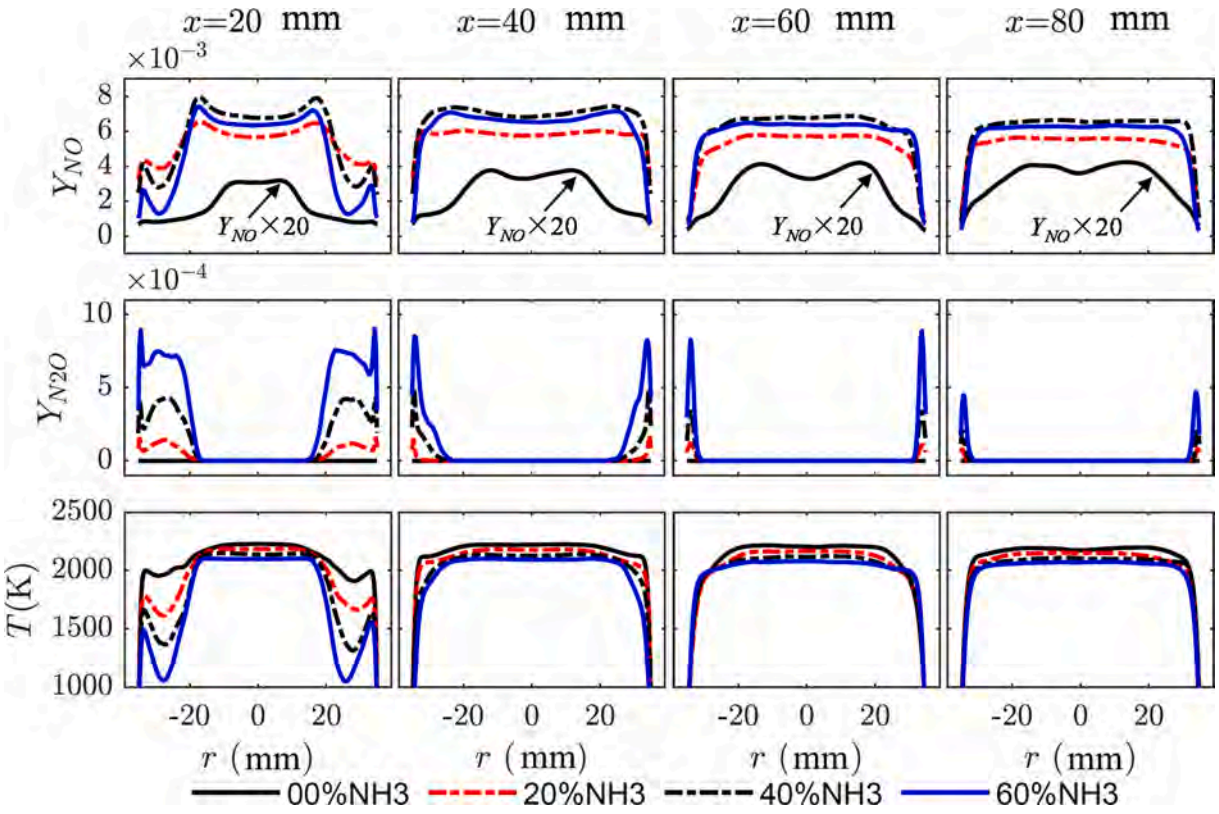

Fig. 15. Species of NO, N_2O and local temperature for different ammonia fraction cases at different axial locations.

visualization area is 70 mm × 140 mm. For 00NH3 shown in Fig. 13 (a), the NO concentration is very low, which is only 104 ppm in simulation STAE value. The numerical result is expanded to 20 times in order to compare with other conditions. It can be seen that the NO is mainly produced in the inner recirculation zone. When $\eta_{NH3} = 20\%$, the emission of NO increases significantly, i.e. to 4351 ppm in simulation. In the section 4.2, it is found that the emission of NO seems to reach its peak value, when the NH_3 fraction is closed to 40%. This can be verified that the NO concentration of the 2D slice for $\eta_{NH3} = 40\%$ is higher than the other cases as shown in Fig. 13.

The distribution of NO is more significant in high stretch zone where the HRR is also high. However, there are some relevance between vortex and NO distribution. Although the phenomenon is not very significant, we cannot ignore it. From Fig. 13, it can be seen that high NO concentration region corresponds with the vortex structure, which is marked by the black box. The NO formation is sensitive to the residence time [40]. While the fluid residence time is increased within the vortex, the local NO formation is high in vortex region. In addition, the NO is also concentrated in the flame surface region, where the heat release rate and the OH concentration is high due to the promotion of the reaction HNO + OH → H_2O + NO [27]. From the macro perspective, the NO is mainly produced in the inner recirculation zone due to the increasing of the residence time within IRZ.

In order to further investigate the residence time of the recirculation zone quantitatively, we plot the axial mean velocity which is shown by black dash line in Fig. 13 (b). The axial velocity value against the × is shown in Fig. 14 (a). The residence time is affected by both the recirculation zone length and the recirculation velocity. For example, the recirculation zone of 00NH3 flame is short and the velocity is high, so that the residence time of 00NH3 flame is small. In this study, the residence time of inner recirculation zone in mean flow field is calculated by:

$$t = \int \frac{1}{U_x} dx \tag{7}$$

t_{res} for each case is given, i.e. $t_{00NH3} = 43.9$ ms, $t_{20NH3} = 44.3$ ms, $t_{40NH3} = 80.0$ ms, $t_{60NH3} = 68.2$ ms. The residence time is decided by the velocity and the length of the recirculation zone. It can be found that the recirculation zone length of ammonia blending cases, i.e·20NH3, 40NH3 and 60NH3 is very close, and longer than 00NH3 condition. So, the determinant reason of residence time is the velocity in the recirculation zone for NH_3 blending cases. We can find that the velocity of 40NH3 condition which is indicated with red line is the lowest, shown in Fig. 14 (a). Besides, we compared the experimental data of velocity, and also found that the recirculation zone velocity of 40NH3 is lowest, which is shown in Fig. 14 (b). The slowest velocity of recirculation zone in case 40NH3 is attributed to combustion speed and flame structure. With the increase of NH_3 ratio, the combustion speed decreases, while with the increase of NH_3 ratio, the flame surface moves inward and the axial partial velocity increases. When the blending ratio of NH_3 is 40%, the velocity in the recirculation zone reaches the minimum. So case 40NH3 has the longest residence time.

It can be seen that, t_{res} is larger with the increasing NH_3 fraction. The residence time reaches peak value at $\eta_{NH3} = 40\%$, while the NO emission also reaches peak value in this condition. The simulation results are consistent with the change trend of NO Therefore, we can conclude that the residence time of inner recirculation zone in mean flow field is corresponding to the NO emission formation.

However, NO concentration is low at outer recirculation zone despite that residence time in this region is long. This indicates that the residence time is not the only reason to influence the NO formation. In fact, temperature and N content in fuel are also key factors affecting NO formation. The temperature in outer recirculation zone and nearby the wall is relatively low, which constitutes the main cause of the low concentration of NO in this region. The influence of temperature and N content will be analyzed in the following section.

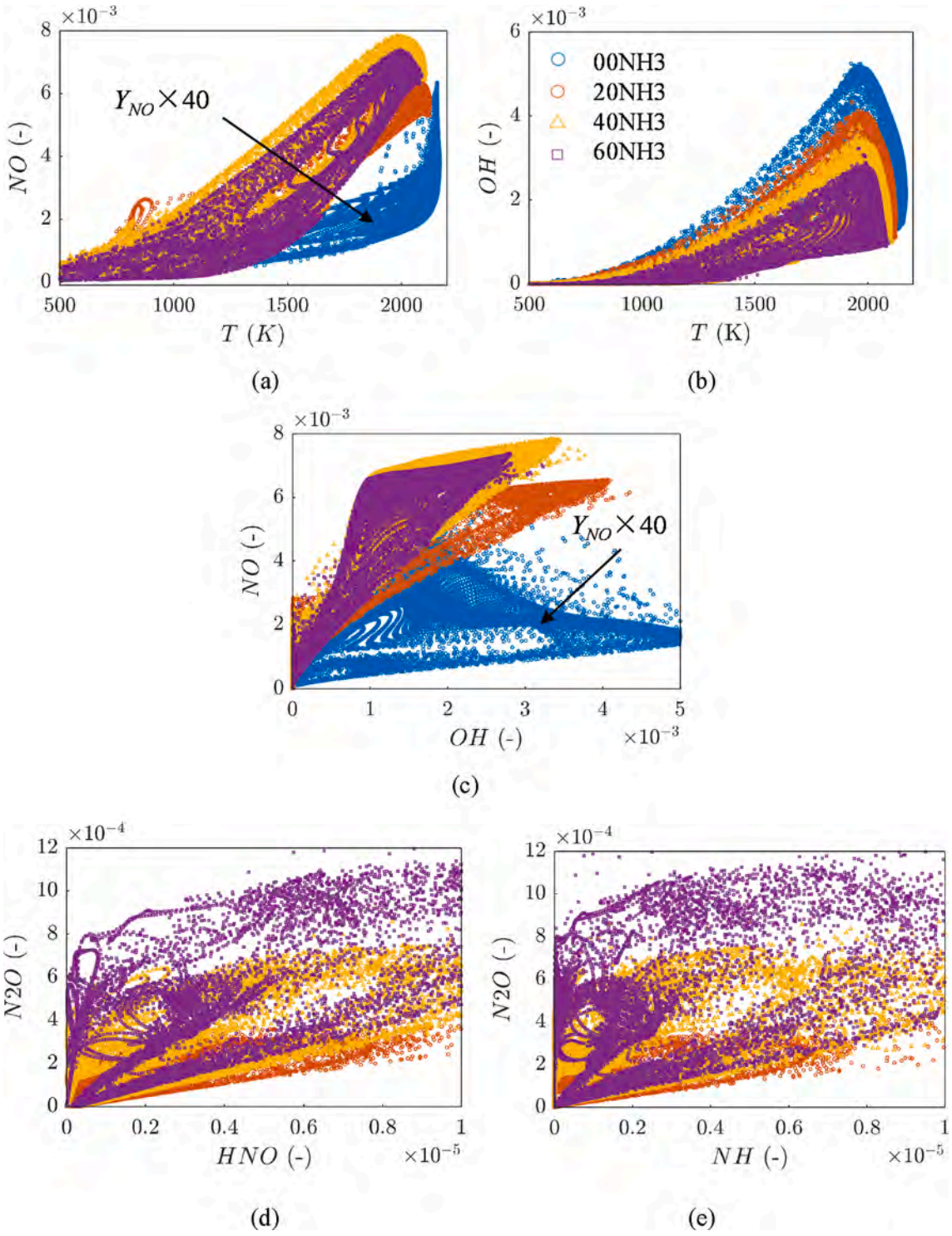

Fig. 16. Correlation of (a) NO-T, (b) OH-T, (c) NO-OH, (d) N_2O-NH and (e) N_2O-HNO for different ammonia fraction cases.

4.4. Analysis of NOx prediction and radical component

Comparison of the mean mass fraction for NO, N_2O emission and temperature along the radial directions at four axial distances (x = 20, 40, 60, 80 mm) for different NH_3 fraction cases are shown in Fig. 15. The NO mass fraction of 00NH3 is amplified 20 times to fit the scale of other conditions. It can be seen that the amount of NO is one order of magnitude larger than N_2O. And the variation trend of NO is opposite with N_2O. NO is mainly distributed in the inner recirculation zone, while N_2O is mainly concentrated in the outer recirculation zone and near wall region. At × = 20 mm, peak NO concentration is demonstrated near to r = ± 20 mm (the flame surface location) and relatively low value is seen near the wall for all cases. The concentration of NO shows a flat profile and N_2O is consumed rapidly in the downstream, i.e. × *greater than 40* mm, for ammonia contained flames. It is also readily seen that ammonia contained flames ($\eta_{NH3} \neq 0$) emit much higher level of NO and N_2O than 00NH3 condition. When NH_3 is blended into the fuel, the nitrogenous components such as NHi and HNO are increasing rapidly, which will promote the formation of fuel-NO through NHi and HNO pathways [20]. Therefore, the fuel-NO emission is one of the important reasons for high

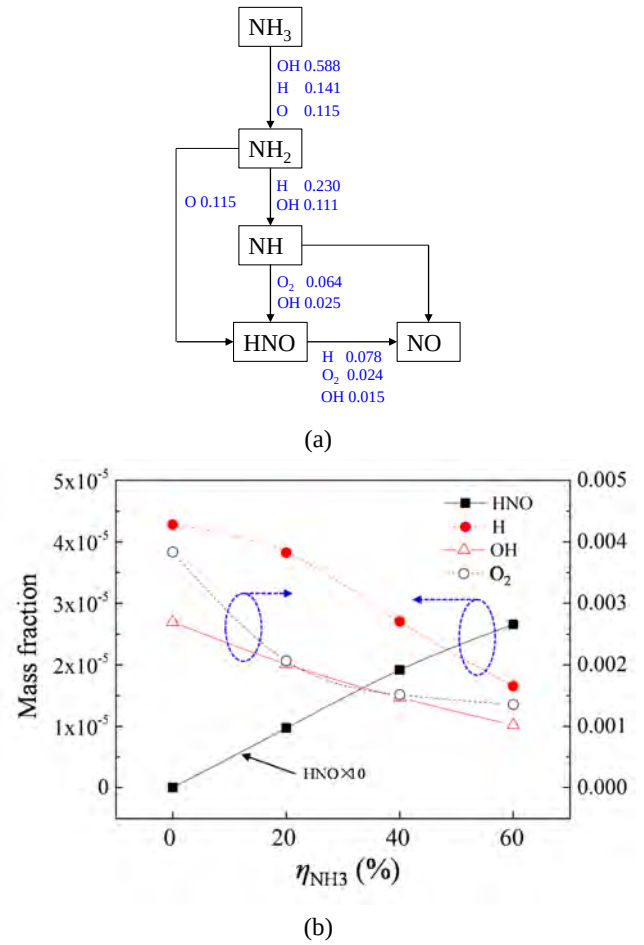

Fig. 17. (a) The reaction path analysis for 40%NH3 case by zero-dimensional calculation in T = 2100 K. (b) the mass fraction of HNO, H, OH and O_2 for different ammonia fraction cases.

NOx emission in CH_4/NH_3/air flames.

The NO value under circumstance of different NH_3 fraction cases is also related to the temperature. These NO is influenced by thermal NO element, which is determined by a set of highly temperature-dependent chemical reactions known as the extended Zeldovich mechanism [41]. In order to further investigate the relationship between NO and temperature, Fig. 16 (a) shows the mass fraction of NO against the temperature. It can be seen that there is a positive correlation between NO and temperature, which is higher for NH_3 blending cases than 00NH3 case. With the increasing of the temperature, the NO value increases and vice versa. Therefore, the high temperature is also one reason to promote the NO formation except for the residence time and nitrogenous components. The content of nitrogenous components in fuel determines the overall level of NO emission. The low temperature in outer recirculation zone and nearby the wall leads to low concentration of NO in specific areas.

Okafor et al. [12,16] found that the local regions of relatively high OH-PLIF intensity and NO-PLIF intensity are correlative in non-premixed CH_4/NH_3/air flames. The positive correlation between NO and OH is also found in current premixed CH_4/NH_3/air flames, which is shown in Fig. 16 (c). In order to further consider the connection between NO and OH, Fig. 16 (b) shows the mass fraction of OH against the temperature, It can be clearly seen that the NO and OH are both positively correlated with the temperature. Therefore, the basic reason for the relevance of NO and OH is that these components are both strongly related to the temperature. The concentration of NO is low in 00NH3 case, so the correlation between NO and OH is not very strong in CH_4/air flames.

N_2O is not obviously correlated with temperature, but has some correlation with NH, shown in Fig. 16 (d). NH radical is a crucial intermediate specie for the formation of N_2O as specified by the reaction NO + NH → N_2O + H [27]. Therefore, the concentration of N_2O can be indicated by the signal of NH-PLIF intensity. Fig. 16 (e) also shows some positive correlation between N_2O and HNO. HNO is a crucial intermediate specie of NO formation, and the NO will further renovate to N_2O [18].

According to the investigation of section 4.2 and 4.3, it can be found that NO will reach peak value at 40%NH3 case. To further reveal the NO formation mechanism, the reaction pathway of 40%NH3 case is analyzed to examine the contribution of the key species in a non-adiabatic condition. This calculation is done with simulation of zero-dimension constant pressure reactor through the self-developed code based on Cantera [42]. The ambient temperature is T = 2100 K which matches the temperature of inner circulation zone. The result is shown in Fig. 17 (a). The value of each product is obtained through the integration of the forward reaction rate until the fuel is consumed 95%, followed with a normalization by dividing the maximum value of reactions. The relative magnitude of the reaction rate is shown by value. It can be seen that the relevant reaction path concerning NO concentration is mainly contributed by HNO, as shown in the reactions below:

$$HNO + H \rightarrow NO + H_2$$

$$HNO + O_2 \rightarrow NO + HO_2$$

$$HNO + OH \rightarrow NO + H_2O$$

The mass fractions of these intermediate species i.e. HNO, H, OH and O_2 for different ammonia fraction cases are shown in Fig. 17 (b). The value of these species is calculated by the space and time-averaged emission (STAE) method from LES results. It can be seen that the concentrations of H, OH and O_2 exhibit a negligible correlation with the NH_3 ratio. Conversely, HNO shows the positive correlation. When NH_3 ratio is low, HNO radicals are near zero because less NH_3 is contained in the fuel. Therefore, reaction rate of HNO are limited, resulting in the low NO value. With the increasing of NH_3 ratio, the concentration of H, O and O_2 decrease while HNO concentration increases. Until the NH_3 ratio is closed to 40%, the concentration of H, OH, O_2 and HNO are all adequate, largely facilitating the NO production. Consequently, the reaction rate of NO is promoted and the NO emission reaches peak value.

5. Conclusions

The emission characteristics of CH_4/NH_3/air co-firing flames in a premixed model combustor are investigated using LES/FGM. The control variables are represented by the progress variance and enthalpy, and the method has been validated to be quite effective and accurate on predicting the premixed CH4/NH3/air flames. The effects of flow and important radical components on emission formation are analyzed. The main conclusion are as follows:

1. The simulation results of flame structure, flow field and emission value match well with experimental measurements. Adding extra NO transport equations will improve the accuracy of emission prediction for ammonia blending flames, then the value of NO, N_2O and O_2 concentration and unburnt fuel is captured well by the LES/FGM method.
2. The nitrogenous components, residence time and temperature are important factors influencing the profile of NO concentration. The content of nitrogenous components in fuel determines the overall high level of NO emission. NO mainly forms in the inner recirculation zone which features long residence time. The global NO level can be estimated by the residence time of the mean IRZ.

3. The distribution of OH and NO is correlative in premixed CH_4/NH_3/air flames. The underlying reason for the relevance is these components are both strongly related to the temperature. It was observed that N_2O is not obviously correlated with temperature, but has a correlation with NH and HNO components.
4. The radical components analysis shows that the relevant reaction path concerning NO concentration is mainly contributed by HNO. With the increase of NH_3 ratio, the concentration of H, O and O_2 decrease while HNO concentration increases. When the NH_3 ratio is closed to 40%, the concentration of H, OH, O_2 and HNO are all adequate. Therefore, the NO production reaches its maximum at $\eta_{NH3} = 40\%$.

CRediT authorship contribution statement

Zhenhua An: Methodology, Data curation, Investigation, Writing - original draft. **Meng Zhang:** Supervision, Writing - review & editing, Formal analysis. **Weijie Zhang:** Methodology, Resources. **Runze Mao:** Data curation, Formal analysis. **Xutao Wei:** Writing - review & editing. **Jinhua Wang:** Writing - review & editing, Supervision. **Zuohua Huang:** Writing - review & editing, Funding acquisition. **Houzhang Tan:** Supervision.

Declaration of Competing Interest

The authors declare that they have no known competing financial interests or personal relationships that could have appeared to influence the work reported in this paper.

Acknowledgements

This study is supported by the National Natural Science Foundation of China (No. 51888103). The authors would like to express their gratitude to Eindhoven University of Technology for Chem1d. Weijie Zhang gratefully acknowledges the generous support from Prof. Jeroen van Oijen during his stay at Eindhoven University of Technology as a visiting student.

References

[1] Ni P, Wang X, Li Hu. A review on regulations, current status, effects and reduction strategies of emissions for marine diesel engines. Fuel 2020;279:118477. https://doi.org/10.1016/j.fuel.2020.118477.
[2] Xiao H, Valera-Medina A, Marsh R, Bowen PJ. Numerical study assessing various ammonia/methane reaction models for use under gas turbine conditions. Fuel 2017;196:344–51.
[3] Kobayashi H, Hayakawa A, Somarathne KDK, Okafor E. Science and technology of ammonia combustion. Proc Combust Inst 2019;37(1):109–33.
[4] Hayakawa A, Arakawa Y, Mimoto R, Somarathne KDKA, Kudo T, Kobayashi H. Experimental investigation of stabilization and emission characteristics of ammonia/air premixed flames in a swirl combustor. Int J Hydrogen Energy 2017;42(19):14010–8.
[5] Valera-Medina A, Marsh R, Runyon J, Pugh D, Beasley P, Hughes T, et al. Ammonia–methane combustion in tangential swirl burners for gas turbine power generation. Appl Energy 2017;185:1362–71.
[6] Li S, Zhang S, Zhou H, Ren Z. Analysis of air-staged combustion of NH3/CH4 mixture with low NOx emission at gas turbine conditions in model combustors. Fuel 2019;237:50–9.
[7] Xiao H, Lai S, Valera-Medina A, Li J, Liu J, Fu H. Study on counterflow premixed flames using high concentration ammonia mixed with methane. Fuel 2020;275:117902. https://doi.org/10.1016/j.fuel.2020.117902.
[8] Fort Belvoir V. Development of an ammonia-burning gas turbine engine. US army engineer research and development laboratories 1996;DA-44-009-AMC-824(T).
[9] Kurata O, Iki N, Matsunuma T, Inoue T, Tsujimura T, Furutani H, et al. Performances and emission characteristics of NH3–air and NH3CH4–air combustion gas-turbine power generations. Proc Combust Inst 2017;36(3):3351–9.
[10] Khateeb AA, Guiberti TF, Zhu X, Younes M, Jamal A, Roberts WL. Stability limits and exhaust NO performances of ammonia-methane-air swirl flames. Exp Therm Fluid Sci 2020;114:110058. https://doi.org/10.1016/j.expthermflusci.2020.110058.
[11] Xiao H, Valera-Medina A, Bowen PJ. Study on premixed combustion characteristics of co-firing ammonia/methane fuels. Energy 2017;140:125–35.
[12] Okafor EC, Somarathne KDKA, Ratthanan R, Hayakawa A, Kudo T, Kurata O, et al. Control of NOx and other emissions in micro gas turbine combustors fuelled with mixtures of methane and ammonia. Combust Flame 2020;211:406–16.
[13] Kurata O, Iki N, Inoue T, Matsunuma T, Tsujimura T, Furutani H, et al. Development of a wide range-operable, rich-lean low-NOx combustor for NH3 fuel gas-turbine power generation. Proc Combust Inst 2019;37(4):4587–95.
[14] Somarathne KDKA, Hatakeyama S, Hayakawa A, Kobayashi H. Numerical study of a low emission gas turbine like combustor for turbulent ammonia/air premixed swirl flames with a secondary air injection at high pressure. Int J Hydrogen Energy 2017;42(44):27388–99.
[15] Somarathne KDKA, Okafor EC, Sugawara D, Hayakawa A, Kobayashi H. Effects of OH concentration and temperature on NO emission characteristics of turbulent non-premixed CH4/NH3/air flames in a two-stage gas turbine like combustor at high pressure. Proceedings of the Combustion Institute. 2020.
[16] Somarathne KDKA, Okafor EC, Hayakawa A, Kudo T, Kurata O, Iki N, et al. Emission characteristics of turbulent non-premixed ammonia/air and methane/air swirl flames through a rich-lean combustor under various wall thermal boundary conditions at high pressure. Combust Flame 2019;210:247–61.
[17] Somarathne KDKA, Colson S, Hayakawa A, Kobayashi H. Modelling of ammonia/air non-premixed turbulent swirling flames in a gas turbine-like combustor at various pressures. Combust Theor Model 2018;22(5):973–97.
[18] Honzawa T, Kai R, Okada A, Valera-Medina A, Bowen PJ, Kurose R. Predictions of NO and CO emissions in ammonia/methane/air combustion by LES using a non-adiabatic flamelet generated manifold. Energy 2019;186:115771. https://doi.org/10.1016/j.energy.2019.07.101.
[19] Ketelheun A, Olbricht C, Hahn F, Janicka J. NO prediction in turbulent flames using LES/FGM with additional transport equations. Proc Combust Inst 2011;33(2):2975–82.
[20] Zhang M, An Z, Wei X, Wang J, Huang Z, Tan H. Emission analysis of the CH4/NH3/air co-firing fuels in a model combustor. Fuel 2021;291:120135. https://doi.org/10.1016/j.fuel.2021.120135.
[21] Zhang W, Karaca S, Wang J, Huang Z, Oijen JV. Large eddy simulation of the Cambridge/Sandia stratified flame with flamelet-generated manifolds: Effects of non-unity Lewis numbers and stretch. Combust Flame 2021;227:106–19.
[22] Zhang M, Wei X, Wang J, Huang Z, Tan H. The blow-off and transient characteristics of co-firing ammonia/methane fuels in a swirl combustor. Proceedings of the Combustion Institute. 2020.
[23] Zhang M, An Z, Wang L, Wei X, Jianayihan B, Wang J, et al. The regulation effect of methane and hydrogen on the emission characteristics of ammonia/air combustion in a model combustor. Int J Hydrogen Energy 2021;46(40):21013–25.
[24] Donini A, Bastiaans RJM, van Oijen JA, de Goey LPH. A 5-D implementation of FGM for the large eddy simulation of a stratified swirled flame with heat loss in a gas turbine combustor. Flow, turbulence and combustion 2017;98(3):887–922.
[25] van Oijen JA. Flamelet-generated, manifolds: development and application to premixed laminar flames. Eindhoven University Press; 2002.
[26] Chem1D A. one-dimensional laminar flame code, Eindhoven University of Technology; 2016.
[27] Okafor EC, Naito Y, Colson S, Ichikawa A, Kudo T, Hayakawa A, et al. Experimental and numerical study of the laminar burning velocity of CH4–NH3–air premixed flames. Combust Flame 2018;187:185–98.
[28] Okafor EC, Naito Y, Colson S, Ichikawa A, Kudo T, Hayakawa A, et al. Measurement and modelling of the laminar burning velocity of methane-ammonia-air flames at high pressures using a reduced reaction mechanism. Combust Flame 2019;204:162–75.
[29] Bouvet N, Halter F, Chauveau C, Yoon Y. On the effective Lewis number formulations for lean hydrogen/hydrocarbon/air mixtures. Int J Hydrogen Energy 2013;38(14):5949–60.
[30] Ketelheun A, Kuenne G, Janicka J. Heat transfer modeling in the context of large eddy simulation of premixed combustion with tabulated chemistry. Flow Turbul Combust 2013;91(4):867–93.
[31] Floyd J, Kempf AM, Kronenburg A, Ram RH. A simple model for the filtered density function for passive scalar combustion LES. Combust Theor Model 2009;13(4):559–88.
[32] Scotti A, Meneveau C, Lilly DK. Generalized Smagorinsky model for anisotropic grids. Phys Fluids A 1993;5(9):2306–8.
[33] Wei X, Zhang M, An Z, Wang J, Huang Z, Tan H. Large eddy simulation on flame topologies and the blow-off characteristics of ammonia/air flame in a model gas turbine combustor. Fuel 2021;298:120846. https://doi.org/10.1016/j.fuel.2021.120846.
[34] Kornev N, Hassel E. Method of random spots for generation of synthetic inhomogeneous turbulent fields with prescribed autocorrelation functions. Commun Numer Methods Eng 2007;23(1):35–43.
[35] Kornev N, Kröger H, Turnow J, Hassel E. Synthesis of artificial turbulent fields with prescribed second-order statistics using the random-spot method. In: PAMM: Proceedings in Applied Mathematics and Mechanics. Wiley Online Library; 2007. p. 2100047–8.
[36] Zhang M, Chang M, Wang J, Huang Z. Flame dynamics analysis of highly hydrogen-enrichment premixed turbulent combustion. Int. J. Hydrogen Energy 2020;45(1):1072–83.
[37] Singh G, Chander S, Ray A. Heat transfer characteristics of natural gas/air swirling flame impinging on a flat surface. Exp Therm Fluid Sci 2012;41:165–76.
[38] Samiran NA, Chong CT, Ng J-H, Tran M-V, Ong HC, Valera-Medina A, et al. Experimental and numerical studies on the premixed syngas swirl flames in a model combustor. Int J Hydrogen Energy 2019;44(44):24126–39.
[39] Dally B, Fletcher D, Masri A. Flow and mixing fields of turbulent bluff-body jets and flames. Combust Theor Model 1998;2(2):193–219.

[40] De Toni A, Hayashi T, Schneider P. A reactor network model for predicting NOx emissions in an industrial natural gas burner. J Braz Soc Mech Sci Eng 2013;35(3):199–206.
[41] He D, Yan W. Influences of different diluents on NO emission characteristics of syngas opposed-flow flame. Int J Hydrogen Energy 2018;43(5):2570–84.
[42] Goodwin DG, Moffat HK, Speth RL. Cantera: An Object-oriented Software Toolkit for Chemical Kinetics, Thermodynamics, and Transport Processes. Version 2.2.0. 2015.